Turkish Journal of Chemistry

Volume 43 | Number 5 Article 6

1-1-2019

Design, synthesis, biological evaluation and molecular docking of novel molecules to PARP-1 enzyme

FATİH TOK

BEDİA KAYMAKÇIOĞLU

RECEP İLHAN

SİNEM YILMAZ

PETEK BALLAR KIRMIZIBAYRAK

See next page for additional authors

Design, synthesis, biological evaluation and molecular docking of novel molecules to PARP-1 enzyme

Authors
FATİH TOK, BEDİA KAYMAKÇIOĞLU, RECEP İLHAN, SİNEM YILMAZ, PETEK BALLAR KIRMIZIBAYRAK, and TUĞBA TAŞKIN TOK

Turkish Journal of Chemistry

http://journals.tubitak.gov.tr/chem/

Research Article

Turk J Chem
(2019) 43: 1290 – 1305

doi:10.3906/kim-1905-15

Design, synthesis, biological evaluation and molecular docking of novel molecules to PARP-1 enzyme

Fatih TOK[1], Bedia KOÇYİĞİT-KAYMAKÇIOĞLU[1,*], Recep İLHAN[2], Sinem YILMAZ[2,3], Petek BALLAR-KIRMIZIBAYRAK[2], Tuğba TAŞKIN-TOK[4]

[1]Department of Pharmaceutical Chemistry, Faculty of Pharmacy, Marmara University, İstanbul, Turkey
[2]Department of Biochemistry, Faculty of Pharmacy, Ege University, İzmir, Turkey
[3]Department of Bioengineering, Faculty of Engineering, University of Alanya Aladdin Keykubat, Antalya, Turkey
[4]Department of Chemistry, Faculty of Arts and Sciences, Gaziantep University, Gaziantep, Turkey

Received: 08.05.2019 • **Accepted/Published Online:** 22.07.2019 • **Final Version:** 07.10.2019

Abstract: Poly (ADP-ribose) polymerase (PARP) enzyme catalyzes the transfer of ADP-ribose into target proteins. Therefore, PARP is responsible for DNA repair, cell proliferation, and cell death. In this study, potential PARP enzyme inhibitors were designed and synthesized. The synthesized compounds were elucidated by Fourier-transform infrared spectroscopy, ^{1}H NMR, ^{13}C NMR, heteronuclear single-quantum correlation, and mass spectrometry, and their purity was checked via thin-layer chromatography, high-performance liquid chromatography, and elemental analysis. A total of 63 newly synthesized compounds were screened in terms of PARP inhibition by cellular PARylation assay in the HeLa cell line. It was found that 19 compounds significantly inhibited the H_2O_2-induced cellular PARylation. The chemosensitizer effect of these compounds in cancer cells treated with doxorubicin (doxo) was investigated. It was found that the combination of potent PARP inhibitors with doxo potentiated a cytotoxic effect, similar to that of olaparib. The results of the molecular docking and absorption, distribution, metabolism, excretion, and toxicity (ADMET) analysis revealed that compound **60** might be classified as a potential PARP inhibitor candidate. Taken together, all of the results suggested that carbohydrazide derivatives could be a promising lead for the treatment for cancer disorders.

Key words: PARP inhibitors, carbohydrazide, urea, molecular docking, ADMET.

1. Introduction

Poly (ADP-ribose) polymerase (PARP) is an important nuclear enzyme that is responsible for the genomic repair, telomerase regulation, transcription, and regulation of cell death. Thus far, 18 members of PARP have been identified. One of which, PARP-1, is the most important enzyme, and consists of 3 dimensional regions: the DNA binding domain, the automodification domain, and the catalytic domain [1,2]. When DNA damage occurs by internal or external factors, PARP-1 activity is stimulated and PARP-1 transfers ADP-ribose subunits from nicotinamide adenine dinucleotide (NAD^+) to nuclear target proteins. Therefore, the DNA damages is repaired and the normal process of the cell continues [3–5].

PARP-1 provides the repair of single-strand breaks (SSBs). If PARP-1 has been damaged, the SSB cannot be repaired, and double-strand breaks can be formed. Eventually, the cells undergo controlled cell death [6,7].

*Correspondence: bedia.kaymakcioglu@gmail.com

The inhibition of PARP-1 activity is the target for anticancer drugs. The inhibition of PARP-1 increases the effect of radiation and chemotherapeutics [8,9]. PARP-1 inhibitors have anticancer activity, especially in BRCA-deficient cells [10]. Furthermore, PARP-1 inhibitors can provide significant benefits against some disorders, such as diabetes mellitus, inflammation, aging, cardiovascular disorders, and neurodegenerative disorders (Parkinsons and Alzheimers) [11–14].

Nicotinamide and 3-aminobenzamide were 1st generation PARP inhibitors. Nowadays, many compounds of PARP-1 enzyme inhibition are in different stages of clinical trials, such as iniparib, rucaparib, veliparib, and olaparib [15]. Structure activity relationships have shown that PARP-1 inhibitors should have 3 structural features: 1) an aromatic ring, 2) a carboxamide moiety, and 3) a side chain. PARP-1 inhibitors try to bind to the PARP-1 catalytic domain with NAD^+ by competition. The CO and NH groups play an important role in interaction with PAR polymers via hydrogen bonds [16]. However, the CO group is not indispensable for inhibition activity, as the C=N group has also demonstrated similar activity. Therefore, the heteroaromatic ring can provide better activity than the aromatic ring [17]. The urea and carbohydrazide groups consist of the CO and NH bond. Islam et al. reported that the hydrazide groups contributed to hydrogen bond interaction with the active side of the enzyme [18].

Through the results obtained in the literature, novel molecules, which contain the urea and carbohydrazide functional groups, were synthesized from methyl-6-aminopyridine-3-carboxylate.

The newly synthesized compounds were screened in terms of PARP inhibition via cellular PARylation assay in the HeLa cell line using the fluorometric method. Meanwhile, all of the compounds were tested for their cytotoxic effects on various cell lines, such as breast, pancreatic, cervical endometrial cancer, and normal lung fibroblast cells. While none of the compounds showed any cytotoxic effect, 19 compounds inhibited the H_2O_2-induced cellular PARylation (even though it was not as strong as the well-known PARP inhibitor, olaparib). PARP enzymes play a critical role in the maintenance of DNA integrity and PARP inhibitors have been shown to possess a chemopotentiating capacity and are able to sensitize cells to chemotherapeutic agents that induce DNA damage [19,20]. Thus, we investigated the chemosensitizer effect of these 19 compounds in cancer cells treated with doxorubicin (doxo), a DNA damaging agent. We found that the combination of potent PARP inhibitors with doxo potentiated cytotoxic effect, similar to that of olaparib.

Aside from the experimental studies, computational methods, including molecular docking, and absorption, distribution, metabolism, excretion, and toxicity (ADMET) analysis, were applied to define the interaction mechanisms of the complexes at a molecular-level and to gain insight on the drug-likeness properties of the compounds for future research about PARP-1.

2. Materials and methods

2.1. Chemistry

All of the chemicals, solvents, and reagents were purchased from Sigma-Aldrich (St. Louis, MO, USA), S D Fine Chemicals (Mumbai, Maharashtra, India) and Merck (Merck KGaA, Darmstadt, Germany). The progress of all of the reactions was monitored via thin layer chromatography (TLC), which was performed on Merck 60 F254 silica gel plates using petroleum ether and ethyl acetate (10:90 v/v) as a solvent system. Chromatograms were visualized under ultraviolet light at 254 nm. Melting points were determined using a Stuart SMP II digital melting point apparatus (Cole-Parmer Ltd. Staffordshire, UK) and were uncorrected. The purities of the synthesized compounds were checked by reversed-phase high-pressure liquid chromatography (HPLC)

(Chromasil C_{18} 4.6 × 150 mm column, 1311A Quat pomp, photodiode array detector) using acetonitrile and water (isocratic flow, 50:50 v/v) as the eluent. The liquid chromatographic system consisted of an Agilent Technologies 1100 series instrument (Santa Clara, CA, USA) equipped with a quaternary solvent delivery system and a model Agilent series G-13158 photodiode array detector. The infrared (IR) spectra were recorded on a Shimadzu 8400 S Fourier-transform infrared spectroscope (Shimadzu Corp., Kyoto, Japan). Proton nuclear magnetic resonance (NMR) (300 MHz) and carbon NMR (75 MHz) spectra were obtained with a Bruker AC-P 200 spectrometer (Bruker Corp., Billerica, MA, USA) using tetramethylsilane (TMS) as the internal standard and deuterodimethylsulfoxide as the solvent. The chemical shift values are given in δ (ppm). The elemental analysis (C, H, N, and S) was performed using CHNS-Thermo Scientific Flash 2000 (Waltham, MA, USA). The electrospray mass spectrometry (ES-MS) data were obtained using an Agilent 1100 series LC/MSD Trap VL&SL spectrometer.

2.1.1. General procedure of urea synthesis

First, 1 mmol methyl 6-aminopyridine-3-carboxylate was solved in acetone, at 80 °C. Isocyanate derivatives in the dry acetone were added in 2 parts. The mixture was refluxed in a water bath. The reaction was screened by TLC. After 8–10 h, the precipitate was filtered off, dried, and purified with ethanol [21].

2.1.2. General procedure of hydrazide synthesis

Hydrazine monohydrate (5 mmol) was added dropwise to a solution of 1 mmol urea compound in ethanol on a magnetic stirrer. The mixture was stirred at room temperature over a period of 8 h. The residue was filtered, washed with water, and dried [22].

2.1.3. General procedure of carbohydrazide synthesis

Benzoyl chloride (1 mmol) derivatives were added dropwise to a solution of hydrazide (1 mmol) in trimethylamine (2 mmol) and dry CH_2Cl_2 (5 mL), at room temperature. The mixture was stirred on a magnetic stirrer over a period of 5 h. Next, the target compounds were washed with distilled water and filtered [23].

The spectrum data of some selected molecules (**16**, **25**, **36**, **42**, **53**, **58**, **60**) from the synthesized compounds is given below; however, all of the chemistry data were also given as supporting information.

1-(5-(2-(4-chlorobenzoyl)hydrazinecarbonyl)pyridin-2-yl)-3-(4-fluorophenyl)urea (16)

Yield: 60%; beige solid, m.p. 265–266 °C; IR (υ, cm^{-1}): 3277, 3171 (N-H); 3043 (aromatic C-H); 1701 (urea C=O); 1660 (hydrazide C=O); 1593, 1554, 1548, 1504, 1445 (C=N, aromatic C=C and C-N); 1211 (C-F); 835 (aromatic C-H bend.). ^{1}H NMR (300 MHz) (dimethyl sulfoxide (DMSO)-d_6/TMS) δ (ppm): 7.19 (t, 2H, C1-H and C3-H, J: 8.4 Hz); 7.55 (t, 2H, C4-H and C6-H, J: 8.4 Hz); 7.61 (d, 2H, C26-H and C28-H, J: 8.8 Hz); 7.70 (d, 1H, C17-H, J: 8.8 Hz); 7.95 (d, 2H, C25-H and C29-H, J: 8.8 Hz); 8.24 (d, 1H, C16-H, J: 8.8 Hz); 8.82 (s, 1H, C14-H); 9.75 (s, 1H, urea NH); 10.21 (s, 1H, urea NH); 10.58 and 10.63 (2s, 2H, hydrazide NH). ^{13}C NMR (75 MHz) (DMSO-d_6/TMS) δ (ppm): 111.03 (C-17), 115.27–115.57 (d, J: 22.50 Hz, C-1 and C-3), 120.66–120.76 (d, J: 7.50 Hz, C-4 and C-6), 121.79 (C-15), 128.43–128.66 (C-26 and C-28), 129.36–129.57 (C-25 and C-29), 131.17 (C-23), 135.05 (d, J: 2.25 Hz, C-5), 146.24 (C-27), 147.27 (C-16), 151.85 (C-9), 155.03 (C-14),

156.22 (C-12), 157.80 (d, J: 237.75 Hz, C-2), 164.08 (C-18), 164.85 (C-22). Anal. calcd. for $C_{20}H_{15}ClFN_5O_3$: C 56.15; H 3.53; N 16.37%. Found: C 57.11; H 3.41; N 15.78%.

1-(5-(2-(4-trifluorobenzoyl)hydrazinecarbonyl)pyridin-2-yl)-3-(4-chlorophenyl)-urea (25)

Yield: 60%; beige solid, m.p. 322–323 °C; IR (v, cm^{-1}): 3336, 3252 (N-H); 3064 (aromatic C-H); 1707 (urea C=O); 1674 and 1643 (hydrazide C=O); 1600 (C=N); 1556, 1494, 1410 (aromatic C=C and C-N); 1240 (C-F); 1097 (C-Cl); 854 (aromatic C-H bend.). ^{1}H NMR (300 MHz) (DMSO-d_6/TMS) δ (ppm): 7.36 (d, 2H, C1-H and C3-H, J: 8.4 Hz); 7.56 (d, 2H, C4-H and C6-H, J: 8.4 Hz); 7.70 (d, 1H, C17-H, J: 8.8 Hz); 7.90 (d, 2H, C25-H and C29-H, J: 7.6 Hz); 8.11 (d, 2H, C26-H and C28-H, J: 7.6 Hz); 8.23 (d, 1H, C16-H, J: 8.8 Hz); 8.81 (s, 1H, C14-H); 9.72 (s, 1H, urea NH); 10.22 (s, 1H, urea NH); 10.66 (b.s., 2H, hydrazide NH). ^{13}C NMR (75 MHz) (DMSO-d_6/TMS) δ (ppm): 111.09 (C-17), 120.40 (C-15), 121.85 (C-4), 122.01 (C-6), 122.28 (C-30), 125.56 (C-26), 125.61 (C-28), 125.92 (C-25), 126.29 (C-29), 128.38 (C-1), 128.73 (C-3), 129.04 (C-27), 131.08–131.93 (C-2), 136.23 (C-5), 137.61 (C-16), 137.73 (C-23), 147.32 (C-14), 151.71 (C-9), 154.95 (C-12), 164.04 (C-18), 164.77 (C-22). Anal. calcd. for $C_{21}H_{15}ClF_3N_5O_3$: C 52.79; H 3.16; N 14.66%. Found: C 53.13; H 2.90; N 13.81%.

1-(5-(2-(4-chlorobenzoyl)hydrazinecarbonyl)pyridin-2-yl)-3-(4-(trifluoromethyl)phenyl)urea (36)

Yield: 60%; beige solid, m.p. 346–347 °C; IR (v, cm^{-1}): 3295, 3230, 3173 (N-H); 3009 (aromatic C-H); 1670 (hydrazide C=O); 1595, 1554, 1537, 1495, 1460 (aromatic C=C and C-N); 1215 (C-F); 839 (aromatic C-H bend.). ^{1}H NMR (300 MHz) (DMSO-d_6/TMS) δ (ppm): 7.58 (d, 2H, C1-H and C3-H, J: 8.4 Hz); 7.67 (d, 2H, C26-H and C28-H, J: 8.8 Hz); 7.74 (t, 3H, C4-H, C6-H and C17-H); 7.93 (d, 2H, C25-H and C29-H, J: 8.8 Hz); 8.25 (d, 1H, C16-H, J: 8.8 Hz); 8.83 (s, 1H, C14-H); 9.80 (s, 1H, urea NH); 10.42 (s, 1H, urea NH); 10.56 (s, 2H, hydrazide NH). ^{13}C NMR (75 MHz) (DMSO-d_6/TMS) δ (ppm): 111.17 (C-17), 118.58 (C-4), 122.14 (C-6), 122.44 (C-15), 122.61 (C-1), 122.86 (C-3), 126.15 (C-7), 126.20 (C-26 and C-28), 128.66 (C-25 and C-29), 129.36 (C-23), 131.16 (C-2), 136.75 (C-16), 137.68 (C-27), 142.49 (C-5), 147.34 (C-14), 151.67 (C-9), 154.75 (C-12), 164.04 (C-22), 164.85 (C-18). Anal. calcd. for $C_{21}H_{15}ClF_3N_5O_3$: C 52.79; H 3.16; N 14.66%. Found: C 51.88; H 3.45; N 15.22%.

1-(5-(2-(4-fluorobenzoyl)hydrazinecarbonyl)pyridin-2-yl)-3-(4-methylphenyl)urea (42)

Yield: 55%; beige solid, m.p. 329–330 °C; IR (v, cm^{-1}): 3255, 3178 (N-H); 3010 (aromatic C-H); 2922 (aliphatic C-H); 1697 (urea C=O); 1668 and 1647 (hydrazide C=O); 1600 (C=N); 1583, 1545, 1485, 1455 (aromatic C=C and C-N); 1095 (C-F); 846 (aromatic C-H). ^{1}H NMR (300 MHz) (DMSO-d_6/TMS) δ (ppm): 2.24 (s, 3H, CH_3); 7.12 (d, 2H, C1-H and C3-H, J: 8.4 Hz); 7.33–7.41 (m, 4H, C25-H, C26-H, C28-H and C29-H); 7.69 (d, 1H, C17-H, J: 8.4 Hz); 7.99 (d, 2H, C4-H and C6-H, J: 8.4 Hz); 8.22 (d, 1H, C16-H, J: 8.4 Hz); 8.80 (s, 1H, C14-H); 9.67 (s, 1H, urea NH); 10.09 (s, 1H, urea NH); 10.53 (s, 2H, hydrazide NH). ^{13}C NMR (75 MHz) (DMSO-d_6/TMS) δ (ppm): 20.33 (C-7), 110.84 (C-17), 115.39–115.68 (d, J: 21.75 Hz, C-26 and C-28), 118.90 (C-15), 128.89 (d, J: 3.00 Hz, C-23), 128.93–129.27 (C-4 and C-6), 130.10–130.12 (d, J: 9.00 Hz, C-25 and C-29), 131.57–131.64 (C-1 and C-3), 136.15 (C-16), 137.02 (C-2), 137.52 (C-5), 147.26 (C-14), 151.80 (C-9), 155.11 (C-12), 164.14 (d, J: 237.75 Hz, C-27), 164.82 (C-18), 165.86 (C-22). Anal. calcd. for $C_{21}H_{18}FN_5O_3$: C 61.91; H 4.45; N 17.19%. Found: C 61.71; H 4.12; N 17.51%.

1-(5-(2-(4-methylbenzoyl)hydrazinecarbonyl)pyridin-2-yl)-3-(4-methoxyphenyl)urea (53)

Yield: 60%; beige solid, m.p. 323–324 °C; IR (υ, cm^{-1}): 3308, 3171 (N-H); 3057 (aromatic C-H); 2999 (aliphatic C-H); 1716 (urea C=O); 1668 (hydrazide C=O); 1593, 1577, 1508, 1479, 1450 (C=N, aromatic C=C and C-N); 1300 (C-O); 844 (aromatic C-H bend.). ^{1}H NMR (300 MHz) (DMSO-d_6/TMS) δ (ppm): 2.36 (s, 3H, CH_3); 3.71 (s, 3H, OCH_3); 6.90 (d, 2H, C1-H and C3-H, J: 8.4 Hz); 7.32 (d, 2H, C26-H and C28-H, J: 8.8 Hz); 7.43 (d, 2H, C4-H and C6-H, J: 8.4 Hz); 7.67 (d, 1H, C17-H, J: 8.8 Hz); 7.82 (d, 2H, C25-H and C29-H, J: 8.8 Hz); 8.22 (d, 1H, C16-H, J: 8.8 Hz); 8.79 (s, 1H, C14-H); 9.66 (s, 1H, urea NH); 10.01 (s, 1H, urea NH); 10.43 (b.s., 2H, hydrazide NH). ^{13}C NMR (75 MHz) (DMSO-d_6/TMS) δ (ppm): 20.99 (C-30), 55.16 (C-7), 110.94 (C-17), 114.05 (C-15), 120.66 (C-4 and C-6), 121.72 (C-1 and C-3), 128.55 (C-26 and C-28), 129.00-129.65 (C-25 and C-29), 131.67 (C-2), 137.48 (C-16), 141.87 (C-27), 147.22 (C-23), 151.86 (C-9), 155.03 (C-14), 155.14 (C-12), 164.13 (C-5), 165.72 (C-18), 171.16 (C-22). Anal. calcd. for $C_{22}H_{21}N_5O_4$: C 63.00; H 5.05; N 16.70%. Found: C 63.08; H 4.93; N 16.40%.

1-(5-(2-(4-nitrobenzoyl)hydrazinecarbonyl)pyridin-2-yl)-3-(4-(methylthio)phenyl)urea (58)

Yield: 70%; beige solid, m.p. 282–283 °C; IR (υ, cm^{-1}): 3313, 3246, 3134 (N-H); 3057 (aromatic C-H); 2901 (aliphatic C-H); 1695 (urea C=O); 1676 and 1643 (hydrazide C=O); 1618 (C=N); 1585, 1548, 1527, 1494, 1427 (aromatic C=C, nitro asym., and C-N); 1390, 1309 (nitro sym. and C-S); 848 (aromatic C-H bend.). ^{1}H NMR (300 MHz) (DMSO-d_6/TMS) δ (ppm): 2.43 (s, 3H, -SCH_3); 7.25 (d, 2H, C1-H and C3-H, J: 8.8 Hz); 7.49 (d, 2H, C4-H and C6-H, J: 8.8 Hz); 7.71 (d, 1H, C17-H, J: 8.0 Hz); 8.14 (d, 2H, C25-H and C29-H, J: 8.4 Hz); 8.21 (d, 1H, C16-H, J: 8.0 Hz); 8.37 (d, 2H, C26-H and C28-H, J: 8.4 Hz); 8.80 (s, 1H, C14-H); 9.74 (s, 1H, urea NH); 10.16 (s, 1H, urea NH); 10.66 (s, 1H, hydrazide NH); 10.87 (s, 1H, hydrazide NH). ^{13}C NMR (75 MHz) (DMSO-d_6/TMS) δ (ppm): 15.72 (C-7), 111.06 (C-17), 119.62 (C-15), 121.69 (C-4 and C-6), 123.79 (C-26 and C-28), 127.54 (C-1 and C-3), 129.00 (C-25 and C-29), 131.18 (C-2), 136.32 (C-5), 137.61 (C-23), 138.06 (C-16), 147.34 (C-27), 149.45 (C-14), 151.72 (C-9), 155.09 (C-12), 164.05 (C-18), 164.37 (C-22). Anal. calcd. for $C_{21}H_{18}N_6O_5S$: C 54.07; H 3.89; N 18.02%. Found: C 53.87; H 4.08; N 17.42%.

1-(5-(2-(4-methylthiobenzoyl)hydrazinecarbonyl)pyridin-2-yl)-3-(4-(methylthio)phenyl)urea (60)

Yield: 60%; beige solid, m.p. 293–295 °C; IR (υ, cm^{-1}): 3308, 3255, 3132 (N-H); 3010 (aromatic C-H); 2918 (aliphatic C-H); 1697 (urea C=O); 1666 and 1639 (hydrazide C=O); 1585, 1543, 1537, 1487, 1473 (C=N, aromatic C=C and C-N); 1309 (C-S); 836 (aromatic C-H bend.). ^{1}H NMR (300 MHz) (DMSO-d_6/TMS) δ (ppm): 2.43 (s, 3H, -SCH_3); 2.51 (s, 3H, C30-H); 7.22 (d, 2H, C26-H and C28-H, J: 8.8 Hz); 7.36 (d, 2H, C1-H and C3-H, J: 8.8 Hz); 7.49 (d, 2H, C25-H and C29-H, J: 8.8 Hz); 7.71 (d, 1H, C17-H, J: 8.8 Hz); 7.86 (d, 2H, C4-H and C6-H, J: 8.8 Hz); 8.23 (d, 1H, C16-H, J: 8.8 Hz); 8.80 (s, 1H, C14-H); 9.77 (s, 1H, urea NH); 10.21 (s, 1H, urea NH); 10.46 and 10.49 (2s, 2H, hydrazide NH). ^{13}C NMR (75 MHz) (DMSO-d_6/TMS) δ (ppm): 14.05 (C-30), 15.74 (C-7), 111.16 (C-17), 119.55 (C-15), 121.94 (C-4 and C-6), 124.97 (C-26 and C-28), 127.55 (C-25 and C-29) 127.93 (C-1 and C-3), 128.38 (C-23), 131.13 (C-2), 136.38 (C-5), 137.71 (C-16), 143.47 (C-27), 147.05 (C-14), 151.76 (C-9), 154.86 (C-12), 164.08 (C-18), 165.34 (C-22. Anal. calcd. for $C_{22}H_{21}N_5O_3S_2$: C 56.51; H 4.53; N 14.98%. Found: C 56.80; H 4.63; N 14.69%.

2.2. Biological studies

2.2.1. Cell culture and compounds treatment

The cell lines used in the biological studies were obtained from the American Type Culture Collection (ATCC, Manassas, VA, USA) and cultured according to the supplier's instructions.

The olaparib was purchased from BioVision (BioVision, Inc., Milpitas CA, USA), while the doxo was obtained from Cell Signaling Technology (Danvers, MA, USA). All of the test compounds and positive controls were prepared as a 1000× stock solution in DMSO to ensure that the final concentration of DMSO was below 0.1%.

2.2.2. Cytotoxicity assay

Cells that were seeded into 96-well plates were treated with the compounds and incubated for 48 h. Cell viability was determined using the Roche WST-1 assay (Roche Group, Basel, Switzerland) according to the manufacturer's instructions. The absorbance was measured using a Varioscan microplate reader (Thermo Fisher Scientific Inc., Waltham, MA, USA) at 440 nm with 690 nm as a reference wavelength. The experiments were done a minimum of 3 times.

For the chemosensitization assay, the HeLa cells were cotreated with a 10-μM dose of the compounds and 1.5-μM dose of doxo, and incubated for 24 h at conventional cell culture conditions. The ratio of surviving cells after the compound treatments was determined again using the WST-1 assay. The experiments were done a minimum of 3 times.

2.2.3. PARylation assay

The PARP inhibitory activity of compounds was investigated by measuring the inhibition of the H_2O_2-induced PARylation in the HeLa cells [24]. Briefly, the HeLa cells, in 96-well black microplates, were pretreated with either potent PARP-1 inhibitors or olaparib for 1 h and then DNA damage was provoked via the addition of a 1-mM dose of H_2O_2 for 10 min. After removal of the supernatant and washing with phosphate buffered saline, the cells were fixed with ice-cold methanol-acetone (7:3) and kept at -20 °C for 20 min. After blocking the cells with 5% bovine serum albumin, the samples were incubated with the primary PAR mAb (Enzo Life Sciences Inc., Exeter, UK) and then with secondary antimouse Alexa Fluor 488 antibody (Thermo Fisher Scientific). The fluorescence values were measured with a fluorometric multiplate reader (Thermo Fisher Scientific). The obtained PAR signal was normalized with a nuclear 4′,6-diamidino-2-phenylindole (DAPI) signal. The experiments were done a minimum of 3 times.

2.3. Computational details

2.3.1. Molecular docking calculations

In order to evaluate the binding sites of a biologically active compound(s) in the target structure, it is crucial to understand the effects of the compound(s) acting as a medical agent. Therefore, molecular docking studies were carried out using Discovery Studio (DS) 2018 software (Dassault Systèmes, Vélizy-Villacoublay, France) [25], which exerts the CDOCKER algorithm [.26]. The crystal structure of target, PARP-1, was obtained from the Research Collaboratory for Structural Bioinformatics Protein Data Bank (http://www.rcsb.org) under PDB ID: 4RV6. This protein model was chosen due to its compatibility with the biological activity studies in this research. All of the synthesized compounds (**1**–**63**), as ligands, were drawn, and the geometry, energy

optimizations were made in vacuum at a DFT/B3LYP/6-31G (d) basis set in Gaussian 09 (Gaussian 09, Revision E.01) software [27]. Additionally, all of the compounds were minimized using the Chemistry at HARvard Macromolecular Mechanics force field [.28], implemented in DS 2018 to determine the ionization states, tautomers, isomers, and conformations of these compounds. Although all of the compounds were prepared, only the molecular docking studies were applied and evaluated on compounds (**56**, **58**, **60**, **61**, and **63**) that showed activity as a result of biological studies in this research.

After preparation of the selected compounds, the enzyme was prepared using DS 2018 tools and minimized until the root mean square deviation (RMSD) reached the lower value of 0.05 kcal/mol $Å^2$. Literature information on PARP-1, and the define and edit binding site tool of DS 2018 were used to determine the binding site of the PARP-1 structures and binding interactions for the compounds.

Prior to the molecular docking process, the docking approach was examined for reliability and accuracy using CDOCKER, GOLD, and Autodock. This stage was applied 3 times to get a most representative searching of the docking calculations. For this reason, the positive control molecule present inside of PARP-1, rucaparib (AG-014699, PF-01367338; RPB), was removed, and then redocking was exerted into the enzyme by self-docking. The RMSD values were used to analyze the reliability of each docking approach with respect to the positive complex (Table 1).

Table 1. RMSD values of the top 3 conformer poses of Rucaparib.

	RMSD		
Pose	CDOCKER	GOLD	AutoDock
1	0.5281	4.6721	1.8435
2	0.4876	5.3846	2.8673
3	0.6835	4.2469	1.9467
Average RMSD (Å)	0.5664	4.7679	2.2192

After validation, CDOCKER was performed between the selected compounds and the enzyme. The docking score, binding energy, and RMSD were used to define the best pose for each complex.

The selected compounds also were investigated with regards to their pharmacokinetic properties using silico ADMET. For this purpose, physicochemical parameters, including solubility, human intestinal absorption (HIA), blood-brain barrier (BBB) penetration, cytochrome P450 (CYP450) 2D6 inhibition (CYP2D6), hepatotoxicity, and plasma protein binding (PPB) were computed using the ADMET subprotocol of DS 2018. The ADMET parameters are depicted in Table 2.

3. Results and discussion

3.1. Chemistry

The urea and carbohydrazide derivatives were synthesized in 3 steps. In the first step, methyl 6-aminopyridine-3-carboxylate was solved in acetone and the urea compounds were synthesized with different substituted isocyanates. In the second step, the ester functional group was converted to the hydrazide group in ethanol with a reflux. In the last step, the carbohydrazide structures were obtained by reacting these hydrazide compounds with substituted benzoyl chloride in dichloromethane (Figure 1 and Table 3). The purity of the synthesized compounds was checked via TLC, melting point, HPLC, and elemental analysis. The structures

Table 2. Drug-likeness properties of the selected compounds and positive controls (doxo and rucaparib for PARP-1).

Compound	Solubility	HIA	BBB level	CYP2D6	Hepatotoxic	PPB
Doxo	2	3	4	false	true	false
Rucaparib	2	0	2	false	true	true
56	2	0	4	false	true	true
58	2	3	4	false	true	true
60	2	0	4	false	true	true
61	2	0	4	false	true	true
63	3	0	4	false	true	true

HIA, human intestinal absorption: 0 = good; BBB, blood-brain barrier: 1 = high, 2 = medium, 3 = low, and 4 = undefined; CYP2D6, with a value of true (inhibitor) or false (no inhibitor); hepatotoxic, with a value of true (toxic) or false (nontoxic); PPB, plasma protein binding, more than 90% for PPB: chemicals strongly bound. Less than 90% for PPB: chemicals weakly bound.

of the synthesized compounds were confirmed by IR, ^{1}H NMR, ^{13}C NMR, heteronuclear single-quantum correlation (HSQC), and MS.

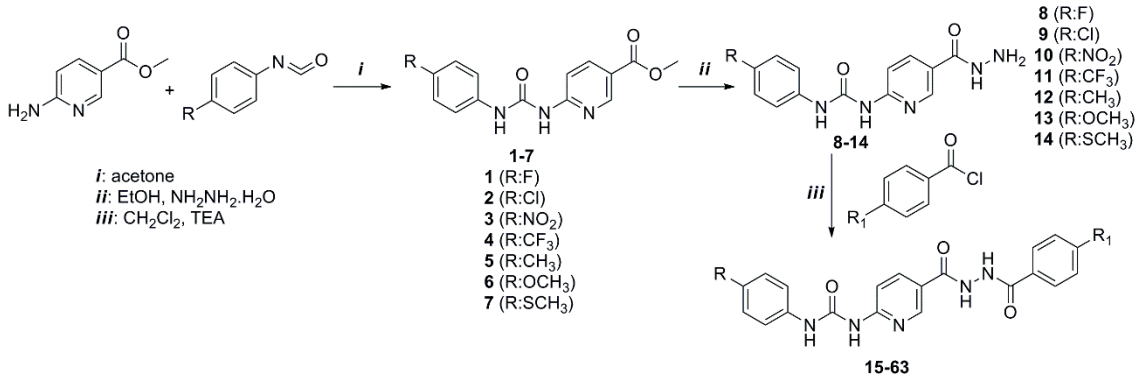

Figure 1. Synthetic pathway of the compounds.

IR spectra of the compounds afforded urea and carbohydrazide N-H stretching (3102–3377 cm^{-1}) and C=O stretching bands (1650–1690 cm^{-1}). Aromatic and aliphatic C-H stretching bands were observed at 3092–3005 cm^{-1} and 3000–2850 cm^{-1}. Aromatic C=C stretching, urea, and carbohydrazide N-H bending bands were found at 1400–1600 cm^{-1}, respectively.

The NH protons of the urea and carbohydrazide groups resonated as a singlet or multiple different singlet peak because of the E/Z isomer at 9.09–11.35 ppm. The metaprotons of the pyridine ring were observed at 7.45–7.78 ppm and the paraprotons of the pyridine ring were observed at 8.21–8.25 ppm as doublet peaks. The ortho protons of the pyridine ring were observed at 8.80–8.82 ppm as a singlet peak. Protons belonging to the aromatic ring and the other aliphatic groups were observed with the expected chemical shift and integral values.

In their ^{13}C NMR spectra, the signal due to the urea and carbohydrazide carbonyl carbon appeared at 161.24–171.93 ppm. The signal due to the aromatic carbon was observed at 153.03–111.67 ppm. C=N carbon on the pyridine ring was observed at 147.0–157.5 ppm. Other aliphatic carbons were observed at the expected regions. The analyses by ES-MS for some selected compounds (**19**, **26**, **46**, **53**, and **61**) showed the presence of

Table 3. The substituents of the carbohydrazide derivatives.

Comp	R	R_1	Comp	R	R_1	Comp	R	R_1
15	F	F	**32**	NO_2	CH_3	**49**	OCH_3	F
16	F	Cl	**33**	NO_2	OCH_3	**50**	OCH_3	Cl
17	F	NO_2	**34**	NO_2	H	**51**	OCH_3	NO_2
18	F	CF_3	**35**	CF_3	F	**52**	OCH_3	CF_3
19	F	CH_3	**36**	CF_3	Cl	**53**	OCH_3	CH_3
20	F	OCH_3	**37**	CF_3	NO_2	**54**	OCH_3	OCH_3
21	F	H	**38**	CF_3	CF_3	**55**	OCH_3	H
22	Cl	F	**39**	CF_3	CH_3	**56**	SCH_3	F
23	Cl	Cl	**40**	CF_3	OCH_3	**57**	SCH_3	Cl
24	Cl	NO_2	**41**	CF_3	H	**58**	SCH_3	NO_2
25	Cl	CF_3	**42**	CH_3	F	**59**	SCH_3	CF_3
26	Cl	CH_3	**43**	CH_3	Cl	**60**	SCH_3	SCH_3
27	Cl	OCH_3	**44**	CH_3	NO_2	**61**	SCH_3	CH_3
28	Cl	H	**45**	CH_3	CF_3	**62**	SCH_3	OCH_3
29	NO_2	F	**46**	CH_3	CH_3	**63**	SCH_3	H
30	NO_2	NO_2	**47**	CH_3	OCH_3			
31	NO_2	CF_3	**48**	CH_3	H			

protonated molecular ion peaks $[M+H]^+$ in agreement with their molecular weight. The major fragmentation pattern involved the cleavage of the urea and carbohydrazide CO-NH amide bond, m/z 178. The elemental analysis of the compounds was given a satisfactory result with the calculated values.

The HSQC spectrum of compound **58** (bearing thiomethyl and nitro substituent) was analyzed to be able to explain the ppm values of the aromatic protons and interaction between the protons and carbons. According to the HSQC spectrum, the interactions between the proton peak at 2.43 ppm and the carbon peak at 15.72 ppm belonged to the thiomethyl group. When the interaction between the proton and carbon on the pyridine ring was examined, the paraproton (C16-H) peak at 8.21 ppm interacted with the carbon peak (C16) at 138.06 ppm. The metaproton (C17-H) peak at 7.71 ppm interacted with the carbon peak (C17) at 111.06 ppm. The peak of C26-H and C28-H was shifted to the downfield by the electron withdrawing effect of the nitro group and appeared at 8.37 ppm, as a doublet, and interacted with the carbon peak (C26 and C28) at 129.00 ppm. The peak of C1-H and C3-H was shifted to the upfield by the electron donating effect of SCH_3 and appeared at 7.25 ppm as a doublet, and interacted with the carbon peak (C1 and C3) at 121.69 ppm. The C4-H and C6-H proton peak at 7.49 ppm interacted with the carbon peak (C4 and C6) at 127.54 ppm. The C25-H and C29-H proton peak at 8.14 ppm interacted with the carbon peak (C25 and C29) at 123.79 ppm.

3.2. Biological evaluation

First, the PARP inhibitory effect of the 63 compounds was evaluated using a 96-well fluorometric cellular PARylation assay, using olaparib as a positive control. In this assay, H_2O_2 treatment was used to induce PARP activity, and as expected, a twice-fold increase was obtained on the cellular PARylation level, which was similar to previous reports [24,29].

When the cells were pretreated with 10 μM olaparib, 1 h prior to H_2O_2 treatment, the cellular PARylation level diminished almost to the nontreated cellular levels. For 19 of the 63 compounds, a concentration of 10 μM of was found to significantly decrease H_2O_2-induced PARylation in the Hela cells (*: P $\leq$ 0.05, **: P $\leq$ 0.001, ***: P $\leq$ 0.005) (Table 4 and Figure 2).

Table 4. Effect of the 63 compounds on H_2O_2-induced cellular PARylation. Data are presented as the mean ± SD.

	PARylation%	SD		PARylation%	SD		PARylation %	SD
No treatment	100	258	+ **20**	195.29	8.49	+ **42**	178.92	5.27
H_2O_2	199.22	7.17	+ **21**	165.25	5.32	+ **43**	185.64	10.38
+ **OLA**	101.96	1.07	+ **22**	206.55	8.95	+ **44**	162.8	8.17
+ **1**	234.98	12.65	+ **23**	215.29	2.75	+ **45**	156.08	6.61
+ **2**	237.57	10.85	+ **24**	219.91	2.75	+ **46**	170.7	7.67
+ **3**	220.28	12.12	+ **25**	221.48	16.2	+ **47**	165.54	9.73
+ **4**	206.36	15.48	+ **26**	201.36	9.24	+ **48**	184.42	2.02
+ **5**	183.69	0.61	+ **27**	208.9	6.08	+ **49**	177.52	10.86
+ **6**	185.39	4.79	+ **28**	163.08	4.35	+ **50**	179.87	6.43
+ **7**	177.31	9.21	+ **29**	198.07	2.73	+ **51**	171.88	9.13
+ **8**	225.69	6.4	+ **30**	185.8	10.15	+ **52**	166.09	14.46
+ **9**	233.39	12.7	+ **31**	223.5	29.05	+ **53**	185.65	15
+ **10**	217.8	16.81	+ **32**	209.01	0.03	+ **54**	179.31	14.88
+ **11**	197.25	14.63	+ **33**	209.88	14.45	+ **55**	164.36	7.2
+ **12**	167.1	6.2	+ **34**	184.06	4.56	+ **56**	184.53	1.18
+ **13**	166.14	9.9	+ **35**	198.1	17.88	+ **57**	193.98	5.53
+ **14**	162.82	14.04	+ **36**	189.21	21.23	+ **58**	133.63	6.02
+ **15**	213.52	9.69	+ **37**	200.59	1.03	+ **59**	166.42	10.23
+ **16**	235.66	12.71	+ **38**	187.94	6.13	+ **60**	160.58	4.81
+ **17**	166.78	11.45	+ **39**	196.71	6.47	+ **61**	150	4.8
+ **18**	195.44	11.32	+ **40**	199.79	3.05	+ **62**	173.94	5.75
+ **19**	209.58	16.44	+ **41**	160.87	6.98	+ **63**	149.71	7.14

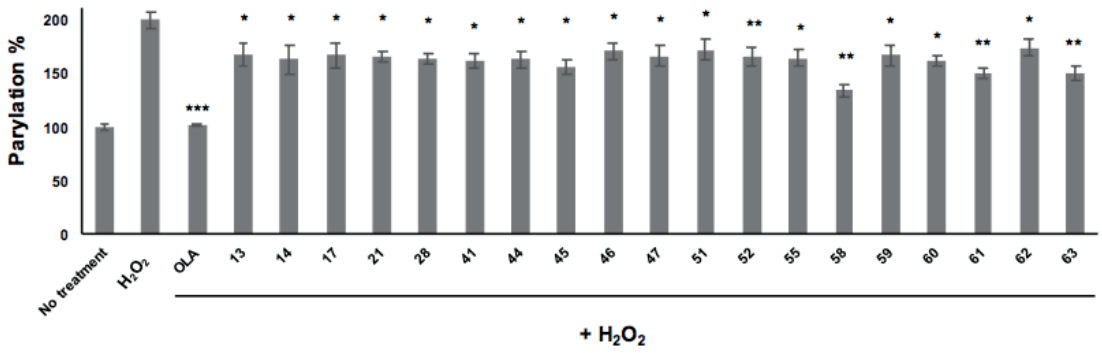

Figure 2. Molecules with promising PARP inhibitor activity seen in the cellular PARylation assay normalized with DAPI signal are presented in the graph. Significance was determined by 2-way ANOVA using GraphPad Prism software (*: P $\leq$ 0.05, **: P $\leq$ 0.001, ***: P $\leq$ 0.005).

The carboxamide group and aromatic moiety are the most important structures for PARP-1 inhibitors. One or more nitrogen/carbonyl-bearing heteroaromatic ring imparting hydrophobic regions at the active side of the enzyme is preferable. At least 1 NH group is necessary for making a hydrogen bond with the enzyme easily. When the hydrophobic groups are attached to the molecule, the inhibitor effect significantly increases. Furthermore, the heteroaromatic ring improves the ability of binding to the enzyme [.30,31]. Therefore, pyridine ring was chosen as the starting material and urea and carbohydrazide functional groups. The biological evaluation showed that electron donating groups, such as a thiomethyl substituent or hydrophobic groups, on the aromatic ring raise inhibitory activity.

Next, the cytotoxicity of these 19 compounds was tested on the HeLa, MCF-7, Capan-1, HCC-1937, and MRC-5 cells, and the data indicated that they had a negligible effect on cell proliferation up to 30 μM. Doxo was used as a positive control and the IC_{50} values of compounds **3**, **10**, and **29**–**34** were given previously. The IC_{50} values of all of the synthesized compounds are given in Table S1 [.32,33].

It has been well-reported that PARP inhibitors function as a chemosensitizer on tumor cells treated with DNA damaging agents. A combination of olaparib and doxo synergistically inhibited proliferation of various cancer cells [24,34] To test whether our putative PARP inhibitors also sensitized DNA damage induced-tumor cells, the HeLa cells were treated with doxo alone or in combination with the compounds of interest. The data suggested that the chemosensitizer effect of compounds **13**, **14**, **21**, **28**, **41**, **44**, **45**, **46**, **47**, **51**, **52**, **58**, **60**, and **63** was statistically significant (Figure 3 and Table 5).

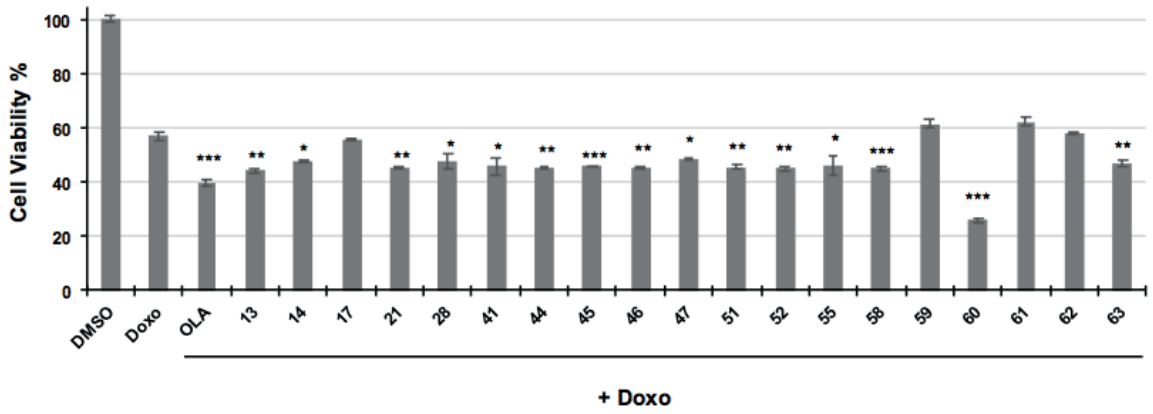

Figure 3. Effect of the compounds on cell viability when combined with doxo is given in the graph. Significance of the differences was determined by 2-way ANOVA (*: $P \leq 0.05$, **: $P \leq 0.001$, ***: $P \leq 0.005$).

DNA damage repair mechanisms are also strongly involved in chemopotentialization. Aside from PARP, other DNA damage response proteins, such as the phosphatidylinositol 3-kinase-related protein kinase family, including DNA-dependent protein kinase, ataxia telangiectasia-mutated and ataxia telangiectasia, and Rad3-related, are also main players of DNA damage response, and inhibition of these proteins is promising as chemopotentiating agents. Furthermore, several other cell signaling molecules play a role in chemosensitization, such as drug transporters, prosurvival proteins, NF-KB pathway members, cell cycle proteins, etc. [35] Our data showed that compound **60** had a very strong chemosensitizer effect that was even better than that of olaparib, suggesting that an additional mechanism(s) aside from PARP inhibition is/are involved, which needs to be further investigated.

Table 5. Chemosensitizer effect of the compounds. Data are presented as the mean ± SD.

	Cell viability %	SD		Cell viability %	SD
DMSO	100	1.33	+ **46**	45.47	0.47
Doxo	57.04	1.65	+ **47**	48.78	0.44
+ **OLA**	39.52	1.07	+ **51**	45.55	0.72
+ **13**	44.33	0.89	+ **52**	44.97	0.69
+ **14**	47.94	0.4	+ **55**	46.26	3.72
+ **17**	55.66	0.66	+ **58**	45.14	0.78
+ **21**	44.98	0.42	+ **59**	61.55	1.68
+ **28**	47.72	2.52	+ **60**	25.97	0.73
+ **41**	45.68	2.81	+ **61**	62.22	1.58
+ **44**	45.15	0.45	+ **62**	58.12	0.3
+ **45**	45.76	0.25	+ **63**	46.95	1.3

3.3. Computational results

In this study, validation of the docking protocol was done by implementing 3 different docking softwares, including CDOCKER, GOLD, and Autodock, according to the manufacturer's instructions. The lowest RMSD value revealed that the crystallographic pose determined the reliability and reproducibility of the docking protocol. Rucaparib was redocked with the lowest RMSD value (0.6 Å) using the CDOCKER method at the best scoring position, as seen in Table 1. These results suggested that the selected docking method was suitable for the experimental results for 4RV6.

3.3.1. Docking results between the compounds (56, 58, 60, 61, and 63) and PARP-1

In the docking studies, the chosen compounds (**56**, **58**, **60**, **61,** and **63**) were used in the same process, based on the positive control (rucaparib). Additionally, their binding affinity was calculated and compared with rucaparib and doxo as PARP-1 inhibitors or PARP-1 positive controls.

The positive control, rucaparib, formed 8 hydrogen bonds with Gly863 (1.839 Å), Ser904 (1.908 Å), Gly863 (1.831 Å), His862 (2.671 Å), Lys903 (2.856 Å), and Glu763 (2.837 Å) residues of the enzyme and 1 halogen with Phe897 (2.806 Å), and 6 hydrophobic interactions with Tyr889, Tyr907, Tyr896, and Ala898 residues. The second, doxo had 10 nonbonding interactions, including 8 hydrogen bonds with Gln759, His862, Tyr889, Asp766, Gly888, Glu763, and Tyr907 residues, and 2 hydrophobic interactions with Met890 and Tyr896 residues of the enzyme. The 3-dimensional (3D) orientations of rucaparib and doxo, and their detail interaction types also are given in Figure S1 and Table S2 of the supporting information section.

The selected compounds, **56**, **58**, **60**, **61**, and **63,** contained methylthio substituent groups in their frame structures that were docked with PARP-1.

Compound **58** had 8 interactions with Tyr907 (2.186 Å), Gly888 (1.768 Å), Asp766 (4.981 Å), Met890 (3.448 Å), Tyr896 (4.138 Å), Leu769 (5.253 Å), Arg878 (3.846 Å), and Ala880 (5.0764 Å) residues in the binding site of PARP-1. On the other hand, compound **60**, which had a very strong chemosensitizer effect that was even better than that of olaparib, displayed 9 nonbonding interactions with different residues (Glu988, Asp766, Met890, Tyr896, Leu769, Arg878, Pro881, and ALA880) of the enzyme. The docking calculations and views showed that, out of all of the docked compounds, the Tyr907 and Tyr896 residues formed the most effective

interactions with compound **58**. The important interactions are also marked in red in Table S2 of the supporting information section.

Aside from interactions of the ligands with PARP-1, their docking orientations were a predominant parameter to define the best one. Compounds **58** and **60** had more fitting orientation than the others (compounds **56**, **61**, and **63**). The relative poses of compound **58** (A) and compound **60** (B), according to doxo (yellow, ball, and stick), in the binding site of PARP-1 are shown in Figure 4. The 2D and 3D orientations of the residues (**56**, **61**, and **63**) and their interaction types are presented in Figure S2 and Table S3 of the supporting information section.

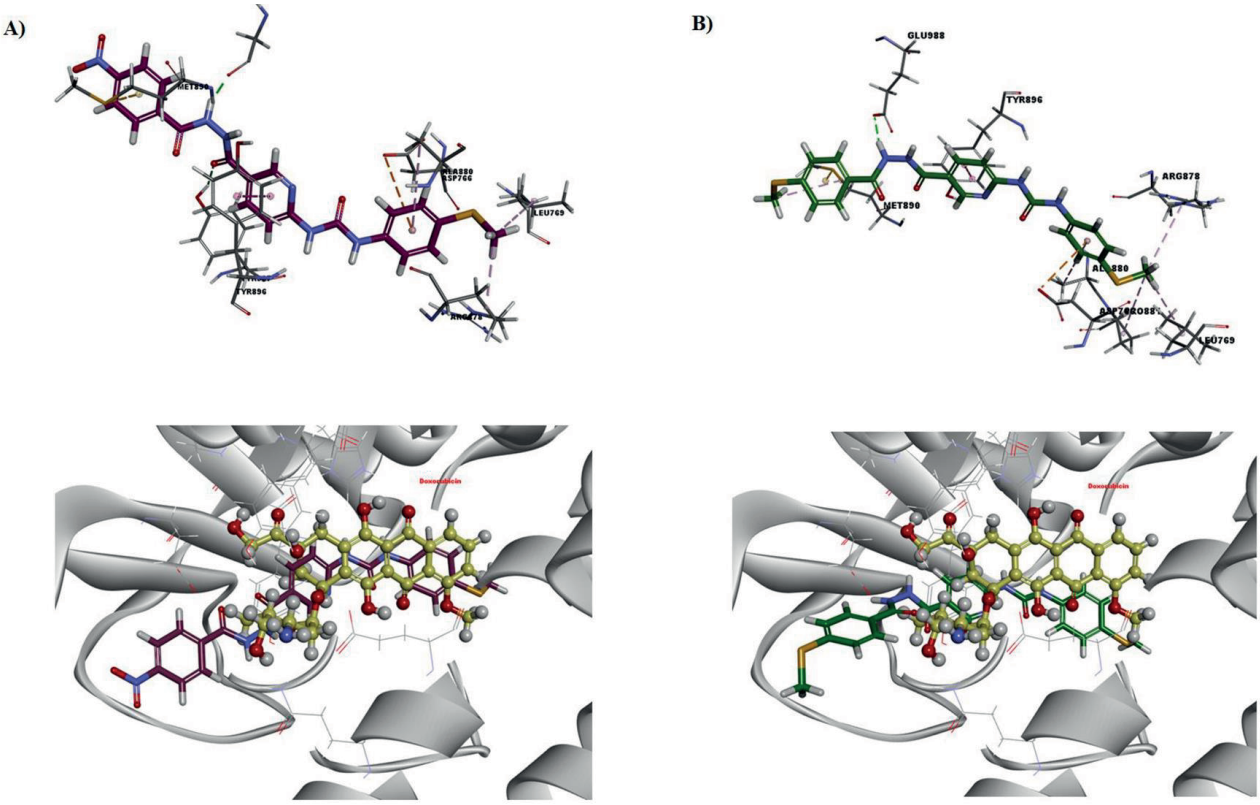

Figure 4. Images of the binding orientations and crucial residues. Figure shows 3D views of the best docked orientations of compounds **58** and **60** with residues in the binding site of the PARP-1.

As mentioned previously, the best poses of the selected compounds were determined based on their docking scores, binding energies, and RMSD values, as demonstrated in Table 6, where it is shown that compounds **58** and **60** had better affinity than the other compounds against PARP-1. These results are marked in red in Table 6.

Furthermore, whether the selected compounds exhibited drug properties or not was examined using ADMET in DS 2018. These results are given in Table 2, which showed that these compounds had low solubility and low BBB permeability. They all also had good human intestinal absorption, except for doxo and compound **58**. Table 2 summarizes that the compounds tended to not be inhibitors against CYPs. Their hepatotoxicity results showed that all of the compounds were toxic to the liver. The final parameter, PPB prediction, demonstrated that all of the compounds had high binding capacity, except for doxo.

Table 6. Binding affinity of the lead compounds. Docking score, binding energy, and RMSD of the PARP-1 positive controls (doxo, rucaparib), and the selected compounds (**56**, **58**, **60**, **61**, and **63**) against the PARP-1.

Compound	Docking score (kcal/mol)	Binding energy (kcal/mol)	RMSD (Å)
Doxo*	–39.7383	–68.7904	0.00989
Rucaparib*	–38.8097	–67.0333	0.00980
56	–21.9615	–59.8692	0.01573
58	–37.1597	–62.6150	0.01567
60	–36.7471	–63.6826	0.01565
61	–21.4600	–61.7469	0.01573
63	–21.5848	–61.2780	0.01574

3.4. Conclusion

In this study, some new PARP-1 inhibitors, containing carbohydrazide and urea derivatives, were designed and synthesized. PARP inhibition of the synthesized compounds was screened by cellular PARylation assay in the HeLa cell line. Of the compounds, 19 demonstrated good enzymatic inhibitory activity, especially those bearing a thiomethyl substituent on the aromatic ring. Compound **58** had the most PARP-1 enzyme inhibitory activity; therefore, compound **58** was selected as a lead compound to be able to develop new PARP inhibitors. Furthermore, the activity of the most potent derivatives was investigated for the chemosensitizer effect of these compounds in cancer cells treated with doxo. Compound **60** had a very strong chemosensitizer effect that was even better than that of olaparib. These results demonstrated that the hydrophobic moieties and electron donating groups were a suitable scaffold for the development of new PARP inhibitors. The results of both the molecular docking and ADMET analyses suggested that compound **60** possessed drug-likeness properties, and according to several criteria, it might be classified as a PARP-1 inhibitor candidate in drug design.

Acknowledgments

This study was supported by the Scientific and Technical Research Council of Turkey (TÜBİTAK) Research Fund under project number: 215S112 and the Marmara University Scientific Research Commission under grant number: SAG-C-DRP-100616-0260.

References

1. Chen Y, Du H. The promising PARP inhibitors in ovarian cancer therapy: from olaparib to others. Biomedicine and Pharmacotherapy 2018; 99: 552-560. doi: 10.1016/j.biopha.2018.01.094
2. Zhu Q, Wang X, Chu Z, He G, Dong G et al. Design, synthesis and biological evaluation of novel imidazo[4,5-c] pyridinecarboxamide derivatives as PARP-1 inhibitors. Bioorganic Medicinal Chemistry Letters 2013; 23 (7): 1993-1996. doi: 10.1016/j.bmcl.2013.02.032
3. Giansanti V, Donà F, Tillhon M, Scovassi AI. PARP inhibitors: New tools to protect from inflammation. Biochemical Pharmacology 2010; 80 (12): 1869-1877. doi: 10.1016/j.bcp.2010.04.022
4. Wang LX, Zhou XB, Xiao ML, Jiang N, Liu F et al. Synthesis and biological evaluation of substituted 4-(thiophen-2-ylmethyl)- 2H-phthalazin-1-ones as potent PARP-1 inhibitors. Bioorganic Medicinal Chemistry Letters 2014; 24 (16): 3739-3743. doi: 10.1016/j.bmcl.2014.07.001

5. Tentori L, Leonetti C, Scarsella M, D'Amati G, Vergati M et al. Systemic administration of GPI 15427, a novel Poly (ADP-ribose) polymerase-1 inhibitor, increases the antitumor activity of temozolomide against intracranial melanoma, glioma, lymphoma. Clinical Cancer Research 2003; 9 (14): 5370-5379. doi: 10.1158/1078-0432.ccr-08-1223

6. Kommoss S, du Bois A, Heitz F, Harter P, Papsdorf M, Ewald-Riegler N. Poly (ADP-ribosyl)ation polymerases: mechanism and new target of anticancer therapy. Expert Review of Anticancer Therapy 2010; 10 (7): 1125-1136. doi: 10.1586/era.10.53

7. Reinbolt RE, Hays JL. The role of PARP inhibitors in the treatment of gynecologic malignancies. Frontiers in Oncology 2013; 3: 1-11. doi: 10.3389/fonc.2013.00237

8. Kroemer G, Castedo M, Saparbaev M, Vitale I, Michels J. Predictive biomarkers for cancer therapy with PARP inhibitors. Oncogene 2013; 33 (30): 3894-3907. doi: 10.1038/onc.2013.352

9. Plummer R. Poly (ADP-ribose) polymerase (PARP) inhibitors: from bench to bedside. Clinical Oncology 2014; 26 (5): 250-256. doi: 10.1016/j.clon.2014.02.007

10. Curtin NJ. Poly (ADP-ribose) polymerase (PARP) and PARP inhibitors. Drug Discovery Today: Disease Models 2012; 9 (2): 51-58. doi: 10.1016/j.ddmod.2012.01.004

11. Szabó C. Cardioprotective effects of poly (ADP-ribose) polymerase inhibition. Pharmacological Research 2005; 52: 34-43. doi:10.1016/j.phrs.2005.02.017

12. Sodhi RK, Singh N, Jaggi AS. Poly (ADP-ribose) polymerase-1 (PARP-1) and its therapeutic implications. Vascular Pharmacology 2010; 53 (3-4): 77-87. doi:10.1016/j.vph.2010.06.003

13. Graziani G, Battaini F, Zhang J. PARP-1 inhibition to treat cancer, ischemia, inflammation. Pharmacological Research 2005; 52 (1): 1-4. doi: 10.1016/j.phrs.2005.02.007

14. Bürkle A, Diefenbach J, Brabeck C, Beneke S. Ageing and PARP. Pharmacological Research 2005; 52: 93-99. doi: 10.1016/j.phrs.2005.02.008

15. Wang J, Tan H, Sun Q, Ge Z, Wang X et al. Design, synthesis and biological evaluation of pyridazino[3,4,5-de]quinazolin-3(2H)-one as a new class of PARP-1 inhibitors. Bioorganic Medicinal Chemistry Letters 2015; 25 (11): 2340-2344. doi: 10.1016/j.bmcl.2015.04.013

16. Giannini G, Battistuzzi G, Vesci L, Milazzo FM, De Paolis F et al. Novel PARP-1 inhibitors based on a 2-propanoyl-3H-quinazolin-4-one scaffold. Bioorganic Medicinal Chemistry Letters 2014; 24 (2): 462-466. doi: 10.1016/j.bmcl.2013.12.048

17. Oliver FJ, Rodríguez MI, Rodríguez-Vargas JM, de Almodovar MR, Linares JL et al. PARP inhibitors: new partners in the therapy of cancer and inflammatory diseases. Free Radical Biology and Medicine 2009; 47 (1): 13-26. doi:10.1016/j.freeradbiomed.2009.04.008

18. Islam R, Koizumi F, Kodera Y, Inoue K, Okawara T, Masutani M. Design and synthesis of phenolic hydrazide hydrazones as potent poly (ADP-ribose) glycohydrolase (PARG) inhibitors. Bioorganic Medicinal Chemistry Letters 2014; 24 (16): 3802-3806. doi: 10.1016/j.bmcl.2014.06.065

19. Calabrese CR, Almassy R, Barton S, Batey MA, Calvert AH et al. Anticancer chemosensitization and radiosensitization by the novel poly (ADP-ribose) polymerase-1 inhibitor AG14361. Journal of the National Cancer Institute 2004; 96 (1): 56-67. doi: 10.1093/jnci/djh005

20. Penning TD, Rodriguez LE, Hristov B,Palma JP, Jarvis K et al. ABT-888, an orally active poly (ADP-ribose) polymerase inhibitor that potentiates DNA-damaging agents in preclinical tumor models. Clinical Cancer Research 2007; 13 (9): 2728-2737. doi: 10.1158/1078-0432.ccr-06-3039

21. Karakuş S, Tok F, Türk S, Salva E, Tatar G et al. Synthesis, anticancer activity and ADMET studies of N-(5-methyl-1,3,4-thiadiazol-2-yl)-4-[(3-substituted)ureido/thioureido] benzenesulfonamide derivatives. Phosphorus, Sulfur and Silicon and the Related Elements 2018; 193 (8). doi: 10.1080/10426507.2018.1452924

22. Altıntop MD, Sever B, Özdemir A, Kucukoglu K, Onem H et al. Potential inhibitors of human carbonic anhydrase isozymes I and II: design, synthesis and docking studies of new 1,3,4-thiadiazole derivatives. Bioorganic and Medicinal Chemistry 2017; 25 (13): 3547-3554. doi: 10.1016/j.bmc.2017.05.005

23. Tok F, Kocyigit-Kaymakcioglu B, Tabanca N, Estep AS, Gross AD et al. Synthesis and structure–activity relationships of carbohydrazides and 1,3,4-oxadiazole derivatives bearing an imidazolidine moiety against the yellow fever and dengue vector, Aedes aegypti. Pest Management Science 2018; 74 (2): 413-421. doi: 10.1002/ps.4722

24. Kırmızıbayrak PB, Ilhan R, Yılmaz S, Gunal S, Tepedelen BE. A Src/Abl kinase inhibitor, bosutinib, downregulates and inhibits PARP enzyme and sensitizes cells to the DNA damaging agents. Turkish Journal of Biochemistry 2018; 43 (2): 101-109. doi: 10.1515/tjb-2017-0095

25. Dassault Systemes Biovia, Discovery Studio Modeling Environment Release DS. Dassault Systemes, San Diego: 2018.

26. Wu G, Robertson DH, Brooks CL, Vieth M. Detailed analysis of grid-based molecular docking: A case study of CDOCKER - A CHARMm-based MD docking algorithm. Journal of Computational Chemistry 2003; 24 (13): 1549-1562. doi: 10.1002/jcc.10306

27. Gaussian 09, Revision E.01, Frisch MJ, Trucks GW, Schlegel HB, Scuseria GE, Robb MA et al. Gaussian, Inc., Wallingford, CT, USA: 2009.

28. Brooks BR, Bruccoleri RE, Olafson BD, States DJ, Swaminathan S et al CHARMM: A program for macromolecular energy, minimization, and dynamics calculations. Journal of Computational Chemistry 1983; 4 (2): 187-217.

29. Szabo C, Brunyanszki A, Szczesny B, Olah G, Coletta C. Regulation of mitochondrial poly (ADP-ribose) polymerase activation by the -adrenoceptor/cAMP/protein kinase A axis during oxidative stress. Molecular Pharmacology 2014; 86 (4): 450-462. doi: 10.1124/mol.114.094318

30. Drenichev MS, Mikhailov SN. Poly(ADP-ribose): From chemical synthesis to drug design. Bioorganic Medicinal Chemistry Letters 2016; 26 (15): 3395-3403. doi: 10.1016/j.bmcl.2016.06.008

31. Jain PG, Patel BD. Medicinal chemistry approaches of poly ADP-ribose polymerase 1 (PARP1) inhibitors as anticancer agents - a recent update. European Journal of Medicinal Chemistry 2019; 165: 198-215. doi: 10.1016/j.ejmech.2019.01.024

32. Tok F, Koçyiğit-Kaymakçıoğlu B, İlhan R, Ballar-Kırmızıbayrak P, Günal S. Design, synthesis and evaluation of biological activities of some new carbohydrazide and urea derivatives. Turkish Journal of Pharmaceutical Science 2018; 15 (3): 304-308. doi: 10.4274/tjps.64935

33. Damanhouri ZA, ElShal MF, Osman A-MM, Bayoumi HM, Al-Harthi SE. Modulation of doxorubicin cytotoxicity by resveratrol in a human breast cancer cell line. Cancer Cell International 2012; 12 (1): 47. doi: 10.1186/1475-2867-12-47

34. Park HJ, Bae JS, Kim KM, Moon YJ, Park SH et al. The PARP inhibitor olaparib potentiates the effect of the DNA damaging agent doxorubicin in osteosarcoma. Journal of Experimental and Clinical Cancer Research 2018; 37 (1): 1-15. doi: 10.1186/s13046-018-0772-9

35. Gupta SC, Kannappan R, Reuter S, Kim JH, Aggarwal BB. Chemosensitization of tumors by resveratrol. Annals of the New York Academy of Science 2011; 1215: 150-160. doi: 10.1111/j.1749-6632.2010.05852.x

SUPPORTING INFORMATION PART OF THE ACTIVITY STUDIES

Table S1: IC_{50} values of all synthesized compounds using human breast cancer cell lines (HCC-1937, MCF-7), human pancreatic adenocarcinoma cell line (Capan-1), normal human lung fibroblast cell line (MRC-5), human servical endometrial carcinoma cell line (HeLa). Doxorubicin was used as standard positive control. (ND: Not determined).

	IC_{50} (μM)				
	HCC1937	**Capan1**	**MCF7**	**HeLa**	**MRC5**
Doxo	1.24 ± 0.48	0.88 ± 0.26	0.875 ± 0.09	1.04 ± 0.31	6.81 ± 0.48
1	ND	ND	ND	ND	ND
2	ND	ND	ND	ND	ND
3	ND	ND	ND	ND	ND
4	25.37 ± 2.52	31.41 ± 4.37	13.48 ± 2.6	14.13 ± 1.1	25.35 ± 2.51
5	ND	ND	ND	ND	ND
6	ND	ND	ND	ND	ND
7	ND	ND	ND	ND	ND
8	ND	ND	ND	ND	ND
9	ND	ND	ND	ND	ND
10	ND	ND	ND	ND	ND
11	ND	ND	ND	ND	ND
12	ND	ND	ND	ND	ND
13	ND	ND	ND	ND	ND
14	ND	ND	ND	ND	ND
15	ND	ND	ND	ND	ND
16	ND	ND	ND	ND	ND
17	ND	ND	ND	ND	ND
18	ND	ND	ND	ND	ND
19	ND	ND	ND	ND	ND
20	ND	ND	ND	ND	ND
21	ND	ND	ND	ND	ND
22	ND	ND	ND	ND	ND
23	ND	ND	ND	ND	ND

24	ND	ND	ND	ND	ND
25	ND	ND	ND	ND	ND
26	ND	ND	ND	ND	ND
27	ND	ND	ND	ND	ND
28	ND	ND	ND	ND	ND
29	7.6 ± 0.09	7.4 ± 0.62	7.3 ± 0.86	6.6 ± 0.53	15.4 ± 1.42
30	10.4 ± 0.6	9.3 ± 0.79	9.6 ± 0.56	9.8. ± 1.86	18.3 ± 1.54
31	7.8 ± 0.82	7.3 ± 0.75	7.5 ± 0.13	7.9 ± 1.68	17.4 ± 1.12
32	ND	ND	ND	ND	ND
33	ND	ND	ND	ND	ND
34	ND	ND	ND	ND	ND
35	ND	ND	ND	ND	ND
36	ND	ND	ND	ND	ND
37	30.2±2.23	ND	ND	24.35±2.40	33.2±2.32
38	ND	ND	ND	ND	ND
39	ND	ND	ND	ND	ND
40	ND	ND	ND	ND	ND
41	ND	ND	ND	ND	ND
42	ND	ND	ND	ND	ND
43	ND	ND	ND	ND	ND
44	ND	ND	ND	ND	ND
45	ND	ND	ND	ND	ND
46	ND	ND	ND	ND	ND
47	ND	ND	ND	ND	ND
48	ND	ND	ND	ND	ND
49	ND	ND	ND	ND	ND
50	ND	ND	ND	ND	ND
51	ND	ND	ND	ND	ND
52	ND	ND	ND	ND	ND
53	ND	ND	ND	ND	ND
54	ND	ND	ND	ND	ND

55	ND	ND	ND	ND	ND
56	ND	ND	ND	ND	ND
57	ND	ND	ND	ND	ND
58	ND	ND	ND	ND	ND
59	ND	ND	ND	ND	ND
60	ND	ND	ND	ND	ND
61	ND	ND	ND	ND	ND
62	ND	ND	ND	ND	ND
63	ND	ND	ND	ND	ND

SUPPORTING INFORMATION PART OF THE COMPUTATIONAL STUDIES

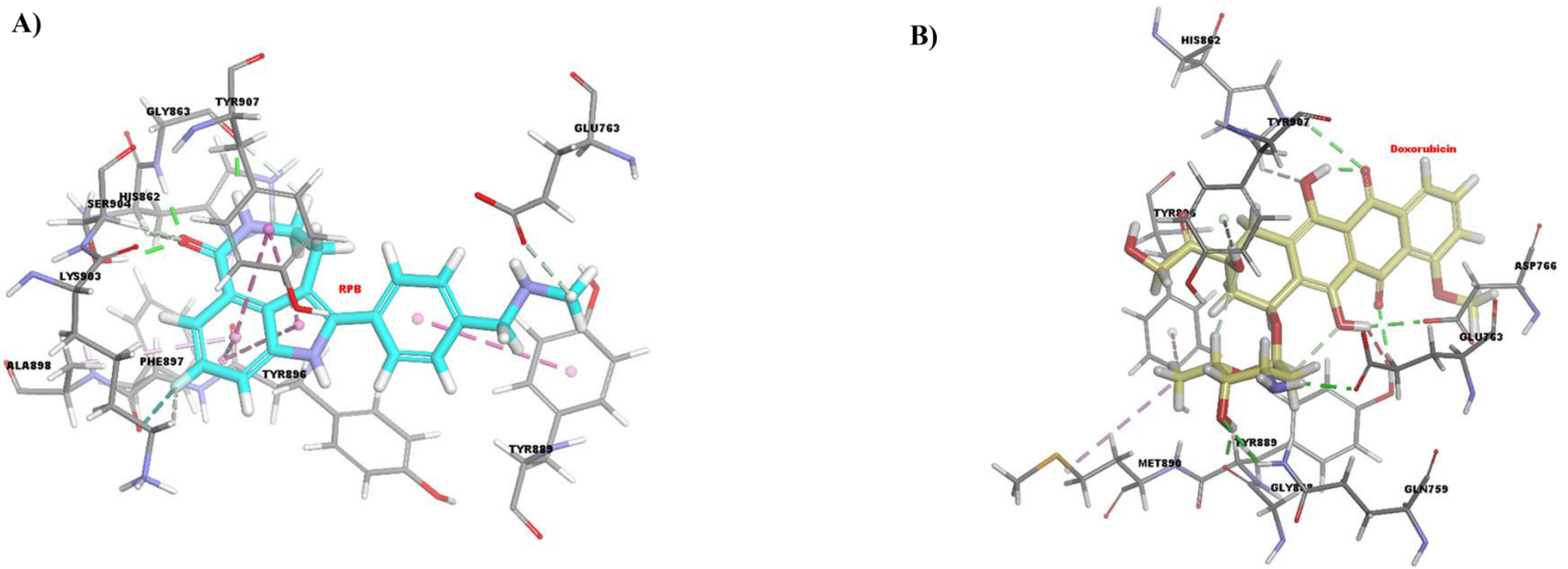

Figure S1. Docked conformation of the positive controls of PARP-1. Figure shows 3D docking poses of **A)** the Rucaparib (light blue, stick) and **B)** Doxorubicin (light yellow, stick) as PARP-1 inhibitors.

Table S2. Interaction types and distance of Rucaparib and Doxorubicin as PARP-1 positive controls and ligands (**58** and **60**) with PARP-1.

Comp. (PARP-1)	Interactions	Distance Å	Bonding	Bonding Types	Bindind site of enzyme	Bindind site of ligand
Rucaparib (RPB)	A:GLY863:HN - A:RPB:O1	1.839	Hydrogen Bond	Conventional Hydrogen Bond	A:GLY863:HN	A:RPB:O1
	A:SER904:HG - A:RPB:O1	1.908	Hydrogen Bond	Conventional Hydrogen Bond	A:SER904:HG	A:RPB:O1
	A:RPB:H1 - A:GLY863:O	1.831	Hydrogen Bond	Conventional Hydrogen Bond	A:GLY863:O	A:RPB:H1
	A:HIS862:HA - A:RPB:O1	2.671	Hydrogen Bond	Carbon Hydrogen Bond	A:HIS862:HA	A:RPB:O1
	A:LYS903:HE2 - A:RPB:F1	2.856	Hydrogen Bond	Carbon Hydrogen Bond	A:LYS903:HE2	A:RPB:F1
	A:SER904:HA - A:RPB:O1	2.539	Hydrogen Bond	Carbon Hydrogen Bond	A:SER904:HA	A:RPB:O1
	A:RPB:H2 - A:GLY863:O	2.975	Hydrogen Bond	Carbon Hydrogen Bond	A:GLY863:O	A:RPB:H2
	A:RPB:H17 - A:GLU763:OE1	2.837	Hydrogen Bond	Carbon Hydrogen Bond	A:GLU763:OE1	A:RPB:H17
	A:PHE897:O - A:RPB:F1	2.806	Halogen	Halogen (Fluorine)	A:PHE897:O	A:RPB:F1
	A:TYR889 - A:RPB	5.701	Hydrophobic	Pi-Pi Stacked	A:TYR889	A:RPB
	A:TYR907 - A:RPB	4.691	Hydrophobic	Pi-Pi Stacked	A:TYR907	A:RPB
	A:RPB - A:TYR907	4.192	Hydrophobic	Pi-Pi Stacked	A:TYR907	A:RPB
	A:TYR896:C,O;PHE897:N - A:RPB	5.069	Hydrophobic	Amide-Pi Stacked	A:TYR896:C,O;PHE897:N	A:RPB
	A:TYR896:C,O;PHE897:N - A:RPB	4.115	Hydrophobic	Amide-Pi Stacked	A:TYR896:C,O;PHE897:N	A:RPB
	A:RPB - A:ALA898	5.241	Hydrophobic	Pi-Alkyl	A:ALA898	A:RPB
Comp.	**Interactions**	**Distance Å**	**Bonding**	**Bonding Types**	**Bindind site of enzyme**	**Bindind site of ligand**
Doxorubicin	A:GLN759:HE21 - Doxorubicin:O37	2.83234	Hydrogen Bond	Conventional Hydrogen Bond	A:GLN759:HE21	Doxorubicin:O37
	A:HIS862:HE2 - Doxorubicin:O20	2.78395	Hydrogen Bond	Conventional Hydrogen Bond	A:HIS862:HE2	Doxorubicin:O20
	A:TYR889:HH - Doxorubicin:O19	2.54788	Hydrogen Bond	Conventional Hydrogen Bond	A:TYR889:HH	Doxorubicin:O19
	Doxorubicin:H53 - A:ASP766:OD2	2.28877	Hydrogen Bond	Conventional Hydrogen Bond	A:ASP766:OD2	Doxorubicin:H53
	Doxorubicin:H60 - A:GLY888:O	1.9483	Hydrogen Bond	Conventional Hydrogen Bond	A:GLY888:O	Doxorubicin:H60
	Doxorubicin:H61 - A:GLU763:OE1	2.14561	Hydrogen Bond	Conventional Hydrogen Bond	A:GLU763:OE1	Doxorubicin:H61
	A:HIS862:HE1 - Doxorubicin:O27	2.52902	Hydrogen Bond	Carbon Hydrogen Bond	A:HIS862:HE1	Doxorubicin:O27
	Doxorubicin:H68 - A:TYR907	2.58467	Hydrogen Bond	Pi-Donor Hydrogen Bond	A:TYR907	Doxorubicin:H68
	Doxorubicin:C36 - A:MET890	5.42442	Hydrophobic	Alkyl	A:MET890	Doxorubicin:C36
	A:TYR896 - Doxorubicin:C36	4.58901	Hydrophobic	Pi-Alkyl	A:TYR896	Doxorubicin:C36

Comp.	Interactions	Distance Å	Bonding	Bonding Types	Bindind site of enzyme	Bindind site of ligand
58	A:TYR907:HH - 58:O28	2.18571	Hydrogen Bond	Conventional Hydrogen Bond	A:TYR907:HH	58:O28
	58:H32 - A:GLY888:O	1.76818	Hydrogen Bond	Conventional Hydrogen Bond	A:GLY888:O	58:H32
	A:ASP766:OD2 - 58	4.98112	Electrostatic	Pi-Anion	A:ASP766:OD2	58
	A:MET890:SD - 58	3.44773	Other	Pi-Sulfur	A:MET890:SD	58
	A:TYR896 - 58	4.13769	Hydrophobic	Pi-Pi Stacked	A:TYR896	58
	58:C48 - A:LEU769	5.25346	Hydrophobic	Alkyl	A:LEU769	58:C48
	58:C48 - A:ARG878	3.84551	Hydrophobic	Alkyl	A:ARG878	58:C48
	58 - A:ALA880	5.07643	Hydrophobic	Pi-Alkyl	A:ALA880	58
Comp.	**Interactions**	**Distance Å**	**Bonding**	**Bonding Types**	**Bindind site of enzyme**	**Bindind site of ligand**
60	60:H32 - A:GLU988:OE2	2.08571	Hydrogen Bond	Conventional Hydrogen Bond	A:GLU988:OE2	60:H32
	A:ASP766:OD2 - 60	4.09083	Electrostatic	Pi-Anion	A:ASP766:OD2	60
	A:MET890:SD - 60	3.45328	Other	Pi-Sulfur	A:MET890:SD	60
	A:TYR896 - 60	4.24352	Hydrophobic	Pi-Pi Stacked	A:TYR896	60
	60:C46 - A:MET890	4.30363	Hydrophobic	Alkyl	A:MET890	60:C46
	60:C50 - A:LEU769	4.81004	Hydrophobic	Alkyl	A:LEU769	60:C50
	60:C50 - A:ARG878	4.75605	Hydrophobic	Alkyl	A:ARG878	60:C50
	60:C50 - A:PRO881	5.04879	Hydrophobic	Alkyl	A:PRO881	60:C50
	60 - A:ALA880	5.01063	Hydrophobic	Pi-Alkyl	A:ALA880	60

Figure S2. 2D and 3D interaction diagrams of compounds. Figure shows compound **56, 61** and **63** (light pink, orange and red color, stick, respectively) with PARP-1 binding domain, forming non-bonding interactions including H-bonds, electrostatics and hydrophobic… etc (different dashed lines) with different residues.

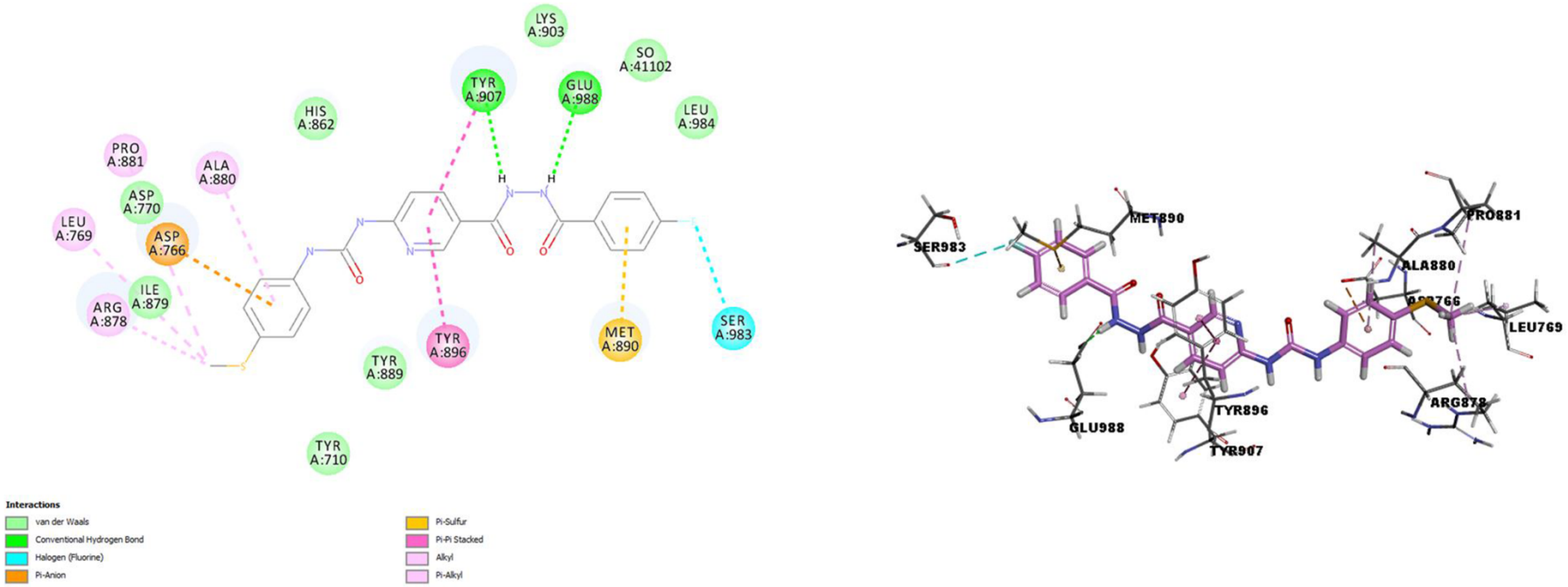

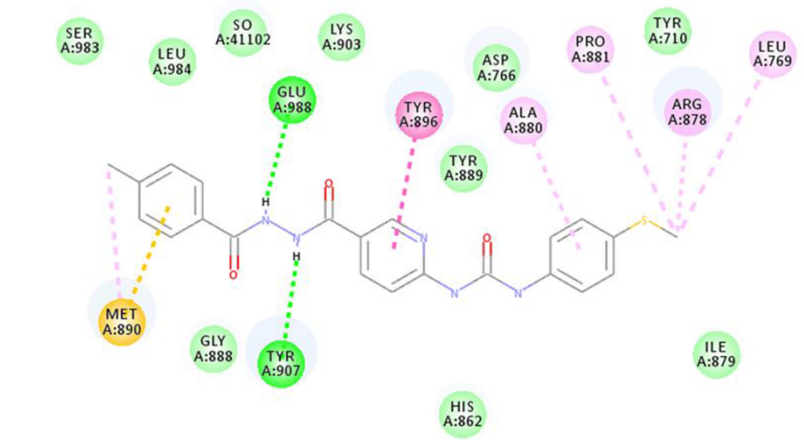
SER A:983
LEU A:984
SO A:41102
LYS A:903
GLU A:988
TYR A:896
ASP A:766
ALA A:880
PRO A:881
TYR A:710
LEU A:769
ARG A:878
TYR A:889
MET A:890
GLY A:888
TYR A:907
HIS A:862
ILE A:879
Interactions
van der Waals
Conventional Hydrogen Bond
Pi-Sulfur
Pi-Pi Stacked
Alkyl
Pi-Alkyl

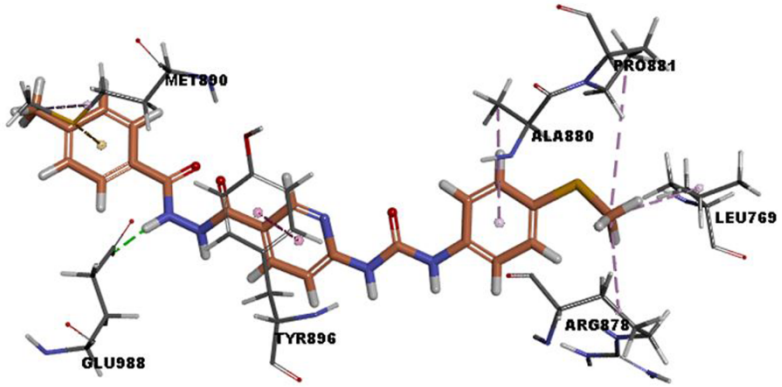
MET890
PRO881
ALA880
LEU769
GLU988
TYR896
ARG878

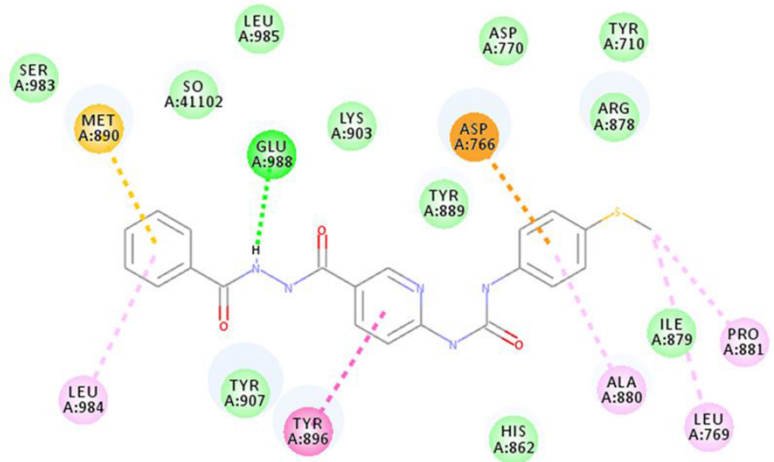

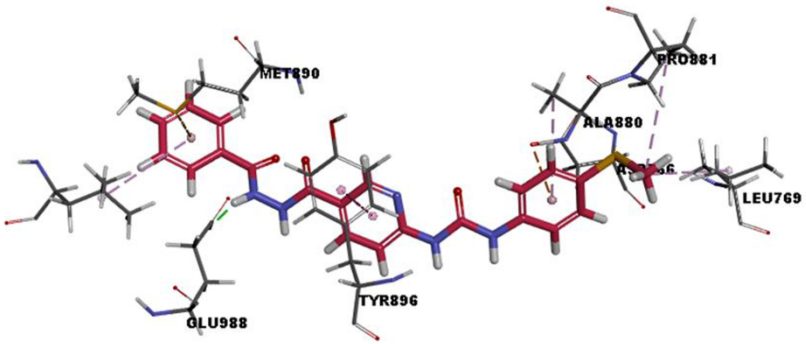

Interactions

- van der Waals
- Conventional Hydrogen Bond
- Pi-Anion
- Pi-Sulfur
- Pi-Pi Stacked
- Alkyl
- Pi-Alkyl

Table S3. Interaction types and distance of of the selected compounds (**56, 61** and **63**) with PARP-1.

Comp.	Interactions	Distance Å	Bonding	Bonding Types	Bindind site of enzyme	Bindind site of ligand
56	56:H32 - A:GLU988:OE2	2.09972	Hydrogen Bond	Conventional Hydrogen Bond	A:GLU988:OE2	56:H32
	A:SER983:O - 56:F41	3.4023	Halogen	Halogen (Fluorine)	A:SER983:O	56:F41
	A:ASP766:OD2 - 56	3.88242	Electrostatic	Pi-Anion	A:ASP766:OD2	56
	A:MET890:SD - 56	3.31055	Other	Pi-Sulfur	A:MET890:SD	56
	A:TYR896 - 56	4.12955	Hydrophobic	Pi-Pi Stacked	A:TYR896	56
	A:TYR907 - 56	5.32726	Hydrophobic	Pi-Pi Stacked	A:TYR907	56
	56:C46 - A:LEU769	5.06907	Hydrophobic	Alkyl	A:LEU769	56:C46
	56:C46 - A:ARG878	4.70033	Hydrophobic	Alkyl	A:ARG878	56:C46
	56:C46 - A:PRO881	5.00127	Hydrophobic	Alkyl	A:PRO881	56:C46
	56 - A:ALA880	4.80613	Hydrophobic	Pi-Alkyl	A:ALA880	56
Comp.	**Interactions**	**Distance Å**	**Bonding**	**Bonding Types**	**Bindind site of enzyme**	**Bindind site of ligand**
61	61:H32 - A:GLU988:OE2	2.07759	Hydrogen Bond	Conventional Hydrogen Bond	A:GLU988:OE2	61:H32
	A:MET890:SD - 61	3.39075	Other	Pi-Sulfur	A:MET890:SD	61
	A:TYR896 - 61	4.05268	Hydrophobic	Pi-Pi Stacked	A:TYR896	61
	61:C45 - A:MET890	4.81517	Hydrophobic	Alkyl	A:MET890	61:C45
	61:C49 - A:LEU769	5.03942	Hydrophobic	Alkyl	A:LEU769	61:C49
	61:C49 - A:ARG878	4.38385	Hydrophobic	Alkyl	A:ARG878	61:C49
	61:C49 - A:PRO881	5.39119	Hydrophobic	Alkyl	A:PRO881	61:C49
	61 - A:ALA880	4.63875	Hydrophobic	Pi-Alkyl	A:ALA880	61
Comp.	**Interactions**	**Distance Å**	**Bonding**	**Bonding Types**	**Bindind site of enzyme**	**Bindind site of ligand**
63	63:H32 - A:GLU988:OE2	1.74954	Hydrogen Bond	Conventional Hydrogen Bond	A:GLU988:OE2	63:H32
	A:ASP766:OD2 - 63	3.72017	Electrostatic	Pi-Anion	A:ASP766:OD2	63
	A:MET890:SD - 63	3.2628	Other	Pi-Sulfur	A:MET890:SD	63
	A:TYR896 - 63	4.05735	Hydrophobic	Pi-Pi Stacked	A:TYR896	63
	63:C46 - A:LEU769	4.98056	Hydrophobic	Alkyl	A:LEU769	63:C46
	63:C46 - A:PRO881	4.73497	Hydrophobic	Alkyl	A:PRO881	63:C46
	63 - A:ALA880	4.85019	Hydrophobic	Pi-Alkyl	A:ALA880	63
	63 - A:LEU984	5.40852	Hydrophobic	Pi-Alkyl	A:LEU984	63